Published in final edited form as:

Nat Neurosci. 2022 July ; 25(7): 876–886. doi:10.1038/s41593-022-01104-7.

A shared disease-associated oligodendrocyte signature among multiple CNS pathologies

Mor Kenigsbuch[1,2,#], **Pierre Bost**[2,3,4,5,#], **Shahar Halevi**[1,2], **Yuzhou Chang**[6,7], **Shuo Chen**[7,8], **Qin Ma**[6], **Renana Hajbi**[9], **Benno Schwikowski**[3], **Bernd Bodenmiller**[5], **Hongjun Fu**[8], **Michal Schwartz**[1,‡,*], **Ido Amit**[2,‡,*]

[1]Department of Neurobiology, Weizmann Institute of Science, Rehovot, Israel.

[2]Department of Immunology, Weizmann Institute of Science, Rehovot, Israel.

[3]Systems Biology Group, Center for Bioinformatics, Biostatistics and Integrative Biology, Institut Pasteur CNRS, Paris, France.

[4]Sorbonne Université, Complexité du vivant, Paris, France.

[5]University of Zurich, Zurich, Switzerland.

[6]Department of Biomedical Informatics, College of Medicine, Ohio State University, Columbus, OH 43210, USA.

[7]Biomedical Sciences Graduate Program, Ohio State University, Columbus, OH 43210, USA.

[8]Department of Neuroscience, College of Medicine, Ohio State University, Columbus, OH 43210, USA.

[9]Department of Molecular Cell Biology, Weizmann Institute of Science, Rehovot, Israel.

Abstract

Alzheimer’s disease (AD) is a complex neurodegenerative disease, perturbing neuronal and non-neuronal cell populations. Here, using single-cell transcritpomics, we mapped all non-immune, non-neuronal cell populations in wild-type and AD model (5xFAD) mouse brains. We identified an oligodendrocyte state that increased in association with brain pathology, which we termed disease-associated oligodendrocytes (DOLs). In a murine model of amyloidosis, DOLs appear long after plaque accumulation, and amyloid-beta (Aβ) alone was not sufficient to induce the DOL signature *in vitro*. DOLs could be identified in a mouse model of tauopathy and in other murine

---

[*] Correspondence should be addressed to: michal.schwartz@weizmann.ac.il (M.S.); ido.amit@weizmann.ac.il (I.A.).

[#] These authors contributed equally to this work.

[‡] These authors jointly supervised this work.

Author contributions

These authors contributed equally: Mor Kenigsbuch, Pierre Bost.

M.S., I.A. and M.K. conceived the study. M.K and P.B. designed the experiments. M.K. conducted the animal work, isolated cells, and generated single-cell sequencing libraries. M.K. and S.H. conducted the imaging experiments. M.K. and S.H. conducted the in vitro experiments with assistance from R.H. P.B. conducted the data analysis for the sequencing, re-analysis of the published datasets and spatial analysis of the mouse LPS treatment Visium data. P.B. developed a new algorithmic approach for image analysis and analyzed and imaging experiments. Y.C., S.C, Q.M., and H.F. conducted the Visium spatial transcriptomics on human brain samples and the data analysis. B.S. and B.B. provided the computational resources for analysis. M.K., M.S., P.B. and I.A. wrote the paper with input from all the other authors.

Competing interests statement

The authors declare no competing interests.

neurodegenerative and autoimmune inflammatory conditions, suggesting a common response to severe pathological conditions. Using quantitative spatial analysis of mouse and postmortem human brain tissues, we found that oligodendrocytes expressing a key DOL marker (SERPINA3N/SERPINA3 accordingly) are present in the cortex in areas of brain damage and are enriched near Aβ-plaques. In postmortem human brain tissue, the expression level of this marker correlated with cognitive decline. Altogether, the present study uncovers a shared signature of oligodendrocytes in central nervous system pathologies.

Editor summary:

We identified an oligodendrocyte signature associated with brain pathology in the 5xFAD model of amyloidosis, which we termed disease-associated oligodendrocytes (DOLs). This signature was found to be shared by oligodendrocytes across pathologies.

Introduction

Alzheimer's disease (AD) is the most common age-related neurodegenerative disease and form of dementia[1,2]. It is considered one of the main public health challenges in Western countries due to population aging. Pathological hallmarks include accumulation of misfolded protein aggregates of Amyloid-Beta (Aβ), collectively known as amyloid plaques, neurofibrillary tangles (NFT) caused by hyper-phosphorylated protein tau[2-4] as well as local brain inflammation[5-8]. Despite intensive research, no disease-modifying therapy has been found, and disease management is complex and inefficient[1,2]. This also applies to other forms of dementia, stressing the need for an in-depth understanding of the cellular and molecular pathways underlying disease onset and progression.

While AD research has been neuron-centric for decades, studies over the last two decades have highlighted the fate of non-neuronal cells and their potential contribution to disease progression. The introduction of single-cell RNA sequencing techniques (scRNA-seq) further advanced the field by uncovering new pathways and cell types associated with the disease, primarily in microglia and astrocytes[9-11]. Oligodendrocytes, which comprise about 20% of all cells in the brain, are the Central Nervous System (CNS) myelin-forming cells. In the context of AD and dementia, significant myelin alterations and breakdown have been observed both in the brain of deceased patients and mouse models[12-14]. Yet, despite their vital function in the brain, it is unclear if and how their fate is altered in AD, and if so, whether it is etiology-dependent or conserved across pathologies.

Using Massively Parallel Single-Cell RNA-seq (MARS-seq), we discovered an oligodendrocyte cell-state arising in 5xFAD mouse model, which we termed Disease-associated Oligodendrocytes (DOLs). By re-analyzing published datasets, we found a similar cell state both in different models of dementia-associated pathology and autoimmune neuroinflammation, indicating this state arises in multiple disease states. Using immunohistochemistry and spatial transcriptomics, we found DOL-like cells in areas enriched with Aβ-plaques in the 5xFAD brain. DOL-like cells were also found in postmortem temporal cortex of AD patients but not in non-demented controls. Overall, our study uncovers that oligodendrocyte response to different CNS pathologies is disease-etiology independent.

Results

Oligodendrocytes display major transcriptomic alteration in the 5xFAD mouse model

Oligodendrocytes are often viewed as passive bystander cells with limited responsiveness to extrinsic cues. Therefore, we were interested to find out if their molecular landscape is altered under AD-associated conditions relative to other non-neuronal cells, which are considered more dynamic. To this end, we performed MARS-seq 2.0[15,16] of non-immune, non-neuronal ($CD45^-$) cells, isolated from whole brains of Wild-Type (WT) and 5xFAD mice (6-8m; n=4 5xFAD, 4 WT, 10-11m; n=3 5xFAD, 4 WT, 15m; n=2 5xFAD, 1 WT), a murine model of amyloidosis carrying 5 familial AD mutations and features a progressive appearance of Aβ-plaques[17] (all the mice characteristics used in this study are described in Supplementary Table 1). Following strict quality controls (Extended data Fig. 1a-c), 10,690 cells were analyzed, and no significant difference in cell library quality was observed between WT and 5xFAD mice (Extended data Fig. 1d). Cells were clustered based on their expression profile using the Pagoda2[18] pipeline, and 17 clusters were detected and annotated based on established cell-type-specific marker genes (Fig. 1a,b and Extended data Fig. 1e). The major populations that were identified were mature myelinating oligodendrocytes (*Plp1, Mbp, Mog*), astrocytes (*Slc1a2*, *Slc1a3*), pericytes (*Myl9*, *Vtn*, *Rgs5*), endothelial cells (*Ly6a*, *Ly6e*), ependymal cells (*Tmem212*, *Ccdc153*) and Choroid plexus epithelium (CP) cells (*Ttr*, *Enpp2*), along with other rarer populations (olfactory ensheathing cells (OEC), fibroblasts, GABA+ neurons). A small contamination by microglia (*Hexb*, *Cx3cr1*) and red blood cells (RBC, *Hbb-bs, Hbb-bt*) was also detected and removed from downstream analysis. Overall, cell-type composition and abundance were not altered in 5xFAD relative to WT (Extended data Fig. 1f).

Next, we performed differential gene expression analysis among cells originating from 5xFAD or WT brains to determine to which extent each cellular population was affected by the disease. To precisely and robustly quantify the number of Differentially Expressed Genes (DEG), we used a binomial regression-based approach that we previously described[19]. Strikingly, we found that mature myelinating oligodendrocytes were the most altered population (adjusted P-value< 0.01) with 98 DEG, while only 25% of the genes were also shared by other cell populations (Fig. 1c,d, DEGs in other cell types are shown in Supplementary Table 2). To validate that this observation was not a result of sampling bias of a high number of oligodendrocytes compared to other cell types, we performed a power analysis. We found that even by sampling 1700 oligodendrocytes (half of their original number), the number of DEG was still higher than other cell types (Fig. 1e). Altogether, these results suggest that in 5xFAD mice, oligodendrocytes display extensive transcriptional alterations.

Identification of a disease-associated oligodendrocyte state

Intrigued by the transcriptional changes observed in mature myelinating oligodendrocytes in 5xFAD mice, we next carried out a deeper molecular characterization of them in

5xFAD relative to WT. To enrich specifically for mature oligodendrocytes, we sorted Galactosylceramidase positive (GalC+)[20] cells (Fig. 2a and Extended data Fig. 2a,b). We sorted cells from 5xFAD mice at different ages ranging from 6 to 24 months and used age-matched WT mice as controls. The sequenced cells were filtered and computationally pooled with the previously sequenced oligodendrocytes, resulting in a database of 13,572 high quality cells (total mice, 6-8m; n=4 5xFAD, 4 WT, 10-11m; n=6 5xFAD, 5 WT, 15m; n=3 5xFAD, 3 WT, 24m; n=4 5xFAD, 4 WT) (Extended data Fig. 2c). Refined clustering analysis of these oligodendrocytes revealed 14 different sub-clusters, each characterized by a unique expression profile (Fig. 2b,c). We further analyzed whether any oligodendrocyte clusters are enriched in 5xFAD relative to WT. This analysis revealed that clusters 12 and 14 were enriched in 5xFAD brains relative to WT (Fig. 2d). Cluster 14, characterized by expression of *Ccl4* and *Lyz2* (Fig. 2b), originated solely from the 24-month-old 5xFAD mice, in which it represented between 9% - 30% of the oligodendrocytes (Extended data Fig. 2d). In contrast, cluster 12 was found at all tested time points from 6 to 8 months and onwards. This cluster represented between 5%–15% of all oligodendrocytes in 5xFAD mice, depending on age, but did not exceed 5% in WT mice (Fig. 2e). This cluster was also distinctly separated from the rest of the oligodendrocytes in the Uniform Manifold Approximation and Projection (UMAP) (Fig. 2c). Because of its significant increase with the disease progression, we termed this transcriptional state “Disease-associated Oligodendrocytes” (DOLs). Interestingly, DOLs were detected long after the appearance of amyloid plaques and inflammation manifestation within the brain in this mouse model of AD[17] (around 9-10-month old). In contrast, Disease-Associated Microglia (DAM) appear as early as 1-2 months after birth in this mouse model[9], highlighting the differential dynamics of response between microglia and oligodendrocytes.

Differential expression analysis between DOLs and the rest of the oligodendrocytes identified 26 genes significantly upregulated by DOLs (adjusted P-value <0.01 and log2 fold change (log2FC)>1, Fig. 2f), encompassing both genes related to immune signaling and non-immune related genes. Immune-related genes included *Serpina3n*, a serine protease inhibitor related to immune proteases[21,22], the complement component *C4b*, several major histocompatibility complex I (MHC-I) genes (H2-D1, H2-K1, *B2m*), and the cytokine *Il33*, which was previously shown to be expressed by oligodendrocytes under acute injury[23]. Among the non-immune upregulated genes, several have been previously linked to neuroinflammation, such as *Klk6*[24], *Sgk1*[25], and the exosome-related CD9 and CD63[26,27]. Of note, similar cells were recently identified by single-nucleus RNA-seq (snRNA-seq)[11] (Extended data fig. 2e,f).

To investigate the signaling pathways and transcriptional circuits possibly controlling the induction of DOLs, we performed motif enrichment analysis for the DEG using iRegulon[28]. The analysis pointed out three major transcription factors (TFs) families: The Stat/Irf (Normalized Enrichment Score, NES=5.4), YY1/NF-κB (NES=6), and Sox9 (NES=6) families (Fig. 2g). MHC-I genes and *C4b* were inferred to be regulated through Stat/Irf and YY1/NF-κB binding motifs, while non-immune genes (*Klk6*, *Sgk1*) were associated with the Sox9 TF, a key regulator of oligodendrocyte differentiation and maturation[29,30]. These results suggest that the DEGs associated with the DOL signature are likely to be induced by a limited set of TF circuits, including members of the NF-κB and Stat/Irf families.

DOLs are independent of dementia's etiology

Since we identified the DOLs in the 5xFAD model, we pondered to what extent the observed signature is amyloidosis-specific, given that the DOLs were detected long after plaques appearance. To this end, we re-analyzed a recently published dataset[31] containing hippocampal cells of WT and of two different mouse models of cognitive impairment, including a model of tauopathy (P301L), which combines tauopathy and amyloidosis (PS2/APP/P301L) (3 animals per group, 19-22 month-old, Fig. 3a). The PS2/APP/P301L mouse model carries mutations in the Presenilin 2 (PSEN2), Amyloid Precursor Protein (APP), and Microtubule Associated Protein Tau (MAPT) genes. Among the 66,002 cells that passed quality control, a first round of analysis allowed identification of a large diversity of brain cells, including highly abundant oligodendrocytes (*Mbp* and *Plp1*, n=30787), microglia (*Cx3cr1* and *Hexb*, n=13508), astrocytes (*Slc1a2*, n=3303), endothelial cells (*Cldn5*, n=3262) , neurons (*Nrgn*, n=2252), Cajal-Retzius (CR) cells (*Reln* and *Nhlh2*, n=1787), T-cells (*Cd3d*, n=1263), pericytes (*Kcnj8*, n=1149), ependymal cells (*Tmem212*, n =841), Vascular smooth muscle cells (*Acta2*, n=455), vascular leptomeningeal cells (*Slc22a6* and Inmt, n=312), neuronal progenitor cells (*Tubb5* and *Smc2*, n=188) and CP epithelial cells (*Ttr*, n=108) (Extended data Fig. 3a,b). The large number of oligodendrocytes in this dataset allowed us to perform a detailed analysis of this compartment, resulting in the identification of 13 different clusters (Fig. 3b). Interestingly, one of those clusters (Cluster 11) was characterized by the upregulation of several characteristic DOL genes, including *Serpina3n* (highest upregulation with log2FC=5.8), *Klk6* (log2FC=4.76), *C4b* (log2FC=3.83), H2-D1 (log2FC=1.7) and *Cd9* (log2FC=1.8) (Fig. 3c). To further validate that this cluster corresponds to DOLs, we performed a gene set enrichment analysis (GSEA). We observed a highly significant enrichment of DOL genes among the upregulated genes of cluster 11 (NES = 1.85, p=1.0e-5) (Fig. 3d), further confirming that those cells are similar to DOLs. In this dataset and in line with our results, DOLs could be barely identified in WT mice but were found both in pure tauopathy (P301L) and a combined tauopathy/amyloidosis model (PS2/APP/P301L), suggesting that DOLs are not specific to the 5xFAD model or amyloidosis (Fig. 3e). Refined analysis of the microglia compartment revealed 11 different clusters, with two of them expressing typical DAM genes such as *Dkk2* and *Cst7* (Extended data Fig. 3c). Of note, DAMs, unlike DOLs, were not found in the model of pure tauopathy (Fig. 3f), highlighting that the oligodendrocytes' response, unlike microglia, is not Aβ-specific.

To further substantiate our finding that DOLs are not induced directly by Aβ accumulation, we generated mouse primary cell cultures of mature-myelinating oligodendrocytes and treated them with $A\beta_{1\text{-}42}$ in different aggregation states- oligomers, fibrils, and plaques[32], followed by RNA-seq. We did not observe upregulation of DOL signature genes following the treatment compared to scramble-treated controls (Fig. 3g, Extended data Fig. 3d), further supporting the contention that Aβ does not lead directly to oligodendrocyte activation or that Aβ is not sufficient. Altogether, the DOL appearance late after Aβ accumulation and lack of response to Aβ *in vitro* suggest that the presence of DOLs in the 5xAD is independent of the primary cause of dementia and might represent oligodendrocytes' response to damage within the CNS.

DOL signature in non-AD pathologies

Based on the above results, we hypothesized that the DOLs identified in amyloidosis and tauopathy models might be found in other chronic CNS pathologies beyond dementia. To test this hypothesis, we conducted a meta-analysis of three previously published mouse scRNA-seq datasets (Fig. 4a). Two of the datasets were from the spinal cord of experimental autoimmune encephalomyelitis (EAE), an experimental model of multiple sclerosis (MS)[33]. MS and EAE are characterized by a massive inflammation resulting from infiltration of adaptive immune cells into the CNS and cytotoxic effect on oligodendrocytes, resulting in their death and de-myelination. EAE is multiphasic, characterized by a phase of gradually worsening symptoms (priming), up to a peak in both inflammation and clinical condition, mostly followed by a reduction in disease severity and inflammation, resulting in improved clinical symptoms (remission)[34]. The first dataset was derived from the spinal cord of mice in the peak stage of EAE[35], compared to spinal cord of control mice injected with Complete Freund Adjuvant (CFA). The second dataset, also from EAE mouse spinal cord, included data from the different phases of EAE: priming, peak and remission, and CFA-injected control[36]. Lastly, the third dataset was generated from the subventricular zone (SVZ) of young (3 months old) and old mice (28-29 months old)[37]. We analyzed these datasets using the Pagoda2 pipeline. All datasets were rich in oligodendrocytes (1207, 2552, and 4683 oligodendrocytes identified, respectively), making them appropriate for our analysis. We first computationally gated oligodendrocytes and looked for differentially expressed genes between pathogenic and non-pathogenic samples (Fig. 4a). In all three datasets, we found expression of pathology-associated genes in oligodendrocytes (Fig. 4b-d), significantly enriched in DOL characteristic genes as revealed by GSEA (Extended data Fig. 4a-c). Interestingly, some variations in the DOL signature were observed across conditions. For instance, *C4b* was upregulated in the acute EAE and aging models, but not in multiphasic EAE, while MHC-I genes were upregulated in both EAE models but not in aging (Fig. 4b-d). We also found that the expression level of DOL signature was linked to EAE disease course; the expression level was elevated during the priming phase, reached its maximum at the peak phase, and gradually reduced during remission (Fig. 4e). These results suggest that the intensity of the oligodendrocyte response correlates with disease severity and likely with the intensity of inflammation.

Non-immune glial cells, mainly astrocytes, were previously reported to respond to systemic inflammation triggered by lipopolysaccharide (LPS) by altering their gene expression, a state described as “reactive astrocytes”[38]. A similar astrocytic profile was also later observed in 5xFAD mouse hippocampus, the disease-associated astrocytes (DAA)[10]. Interestingly, DAA and DOLs transcriptomic signatures partially overlap, as both include *Serpina3n*, H2-D1, *B2m,* and *C4b* genes. A recently published study investigated the spatial transcriptome of mouse brain sections following systemic LPS injection using Visium platform from 10x Genomics[39]. We were intrigued whether in this experimental setting a DOL-like response is induced, as we found in the neuroinflammatory settings in the mouse brain and test its co-localization with oligodendrocytes markers. We first performed an un-supervised demultiplexing of the data using topic modeling (Methods): using this approach, we identified a topic (topic number 8), i.e., a latent dimension, that was strongly expressed in the LPS-stimulated samples (S1, S2, and S6) but not in control samples (S3, S4, and

S7) (Extended data Fig. 4d). Importantly, the genes most significantly contributing to this dimension included several members of the DOL signature (Extended data Fig. 4e), prompting us to call this dimension the DOL-like signature. *Serpina3n* expression was significantly higher in LPS-treated mice compared with control animals (Extended data Fig. 4f). Spatially, the DOL-like response was observed in regions surrounding the 3rd and lateral ventricles, suggesting factors carried by the cerebrospinal fluid (CSF) might be, at least partially, mediating this response (Fig. 4f). We examined if the observed DOL-like topic is associated with oligodendrocytes topic. We identified topic number 2 as enriched in oligodendrocyte markers (high contribution of *Plp1*, *Mbp,* and *Mog* genes), and its spatial pattern across sections corresponded to the expected spatial distribution of white matter (Extended data Fig. 4g). Correlation between the intensity of the two topics was low (R^2 =0.0017), suggesting that the DOL-like signature also included the response of other cell types. Indeed, among the top genes contributing to this topic we found several markers of astrocyte activation such as *Gfap* and *Gja1*, suggesting that the DOL-like response is also shared by activated astrocytes in systemic LPS challenge.

Our meta-analysis further substantiated the notion that the DOL response is a conserved response of oligodendrocytes to pathological deviation from CNS homeostasis, which might be relevant to multiple diseases beyond AD. Furthermore, the overlap between the signatures of DOLs and of reactive astrocytes suggests a common response module of non-immune glia.

Spatial analysis of DOLs in mouse and human brain sections

Next, we studied the spatial distribution of DOLs in the mouse model of amyloidosis, the 5xFAD brain. As a proxy to the DOL signature, we used the protein marker SERPINA3N, encoded by the most prominent gene associated with the DOL state, *Serpina3n*. We first analyzed by immunofluorescence and confocal microscopy coronal sections from 16-month-old 5xFAD mouse brains stained for OLIG2 (oligodendrocyte-lineage nuclear marker), SERPINA3N, and human Aβ (amyloid plaques). We found $OLIG2^+SERPINA3N^+$ double-positive cells (Fig. 5a, Extended data Fig. 5a, white arrows) in areas of damage (enriched with Aβ-plaques), while no SERPINA3N signal was observed in the WT brain. To perform an extensive and quantitative spatial analysis, we used the same cohort of 16-month-old 5xFAD (n=4) and WT (n=2) mice, stained coronal brain sections for OLIG2 as well as for SERPINA3N and Aβ plaques, and analyzed them by scanning a large area (on average 11.5 mm^2) of the cerebral cortex, using a slide scanner. To automatically detect cells, we used the recently published tool DeepCell[40]. Plaques were detected using a classical watershed-based segmentation approach (Methods) (Fig. 5b). A total of 309,333 cells were analyzed. To validate the method used for the analysis, we performed quality controls, which ruled out bias of cell size or OLIG2 intensity across samples (Extended data Fig. 5b,c). By automated thresholding, we confirmed a highly homogeneous proportion of $OLIG2^+$ cells across samples (Extended data Fig. 5d,e) and a limited number of false-positive Aβ plaques detected in the WT (<50) (Extended data Fig. 5f). We then proceeded to analyze SERPINA3N immunoreactivity. Automated thresholding of SERPINA3N intensity (Extended data Fig. 5g) revealed a high frequency of $SERPINA3N^+$ cells in 5xFAD mice but not in WT (Fig. 5c), a pattern that could also be observed among $OLIG2^+$ cells (Fig. 5d).

To assess the spatial distribution of OLIG2$^+$SERPINA3N$^+$ cells, we computed the Besag's L function[41] of these cells in each of the examined 5xFAD brains (Fig. 5e). Briefly, the L function describes the mean number of pairs of points (i.e., pairs of OLIG2$^+$SERPINA3N$^+$ cells) at a given radius (r). For a given r, a positive or negative value corresponds to a 'higher than expected' or 'lower than expected' number of pairs, respectively, compared to a random spatial distribution. We observed highly similar profiles across the four tested brains, with positive values of the L function between 10 and 300 μm, with a peak around 50-70 μm, validating that OLIG2$^+$SERPINA3N$^+$ cells are not randomly distributed across the cortex but appear in discrete areas. Such a distribution of OLIG2$^+$SERPINA3N$^+$ cells argued in favor of association of these cells with tissue damage and prompted us to examine their spatial association with areas of plaques, which are known to be the sites of damage in this model[42-46].

To examine the association between OLIG2$^+$SERPINA3N$^+$ cells and plaques, we fitted a penalized spatial Gibbs point pattern model, termed PenGE[47]. Briefly, we provided a list of range values (30, 80, 160, and 300μm), and PenGE estimated the most likely potential-energy function between subjects of interest, under the form of a stepwise function, where a positive value corresponds to an 'attraction' and a negative value to 'repulsion'. After also verifying by this analysis that OLIG2$^+$SERPINA3N$^+$ cells are not randomly distributed (Fig. 5f, blue), we analyzed the spatial interaction between OLIG2$^+$SERPINA3N$^+$ cells and plaques. We found a positive interaction in ranges below 30μm (Fig. 5f, red) in all tested brains. This analysis, therefore, suggests that the spatial distribution of OLIG2$^+$SERPINA3N$^+$ cells could be linked to damage areas (enriched with plaques).

While mouse oligodendrocytes with a similar transcriptomic signature to DOLs were previously identified using snRNA-seq, no evidence of such cells was reported in humans using the same technique[11,48]. Indeed, snRNA-seq was shown to have lower sensitivity, rendering it unsuitable for detecting many activation-related genes[49]. To further examine whether DOL signature could be relevant to human AD, we re-analyzed spatial transcriptomic data of postmortem human brain sections from the middle temporal gyrus[50]. Similar to the analysis of the mouse Visium samples, we performed a topic modeling approach and identified two topics that were specifically expressed by one of the two AD samples (Fig. 5g). Analysis of the most contributing genes revealed that the first topic was associated with macrophage and microglia-specific genes (*C1QC, C1QA, AIF1,* and *FCER1G*) (Extended data Fig. 5h), while *SERPINA3* was the most contributing gene of the second topic, together with several inflammatory genes such as *CHI3L1, VSIG4,* and *SOD2* (Extended data Fig. 5i). The macrophage signature displayed a highly clustered pattern (Fig. 5h, middle panel), while the inflammatory topic was more spatially dispersed (Fig. 5h, right panel). The inflammatory topic intensity was higher in the margins of high-macrophage regions. These results suggested that the expression of DOL key genes, such as SERPINA3, could be relevant in human AD.

To detect oligodendrocytes that express key features of DOLs in human AD, we analyzed by immunohistochemistry postmortem brain samples from AD patients (n=8) and age-matched non-demented controls (NDC, n=8). The patients' disease description is shown in Supplementary Table 3. We have imaged a $20 mm^2$ area of the temporal cortex, containing both grey matter (GM) and white matter (WM). As in the mice, we used SERPINA3 (the human homolog of SERPINA3N) and CC1, an oligodendrocyte specific marker[51], together with Thioflavin-S (intra- and extracellular Aβ). Confocal imaging revealed the presence of $SERPINA3^+CC1^+$ cells in the GM of the temporal cortex of postmortem AD patients but not in NDC (Fig. 5i, Extended data Fig. 5j). To quantify the incidence of $SERPINA3^+$ cells, we applied the same approach as for the mouse sections, using our image analysis pipeline (Fig. 5b; Extended data Fig. 5k), and a total of 475,091 cells were analyzed. Automatic thresholding of SERPINA3 intensity (Extended data Fig. 5l) confirmed the significant enrichment ($p=0.027$) of $SERPINA3^+$ cells in postmortem AD compared to NDC sections (Fig. 5j). Interestingly, we observed a significant correlation ($p=0.0043$ and $R^2=0.50$) between the proportion of $SERPINA3^+$ cells and the Mini-Mental State Examination (MMSE) score (Fig. 5k), suggesting that SERPINA3 might serve as a quantitative marker of AD-induced cognitive impairment.

Overall, using spatial transcriptomics and immunohistochemistry, we identified SERPINA3N and SERPINA3 in mice and humans, respectively, as key markers of non-immune glia activation in AD.

Discussion

In this work, using scRNA-seq, we identified an oligodendrocyte cell state (disease-associated oligodendrocytes, DOLs) that represent a shared transcriptomic module emerging in response to deviation from CNS homeostasis. This transcriptomic module seems to be common across different pathological states, and elements of it are potentially relevant to human diseases.

In the 5xFAD mouse model of amyloidosis, DOLs appear around ten months of age, following numerous pathological events that occur earlier in the brains of these mice, including Aβ-plaque accumulation, gliosis, inflammation, and cognitive impairments[17]. These results suggest that the oligodendrocyte response to damage in 5xFAD is late relative to other non-neuronal cells, such as microglia and astrocytes[9,10], indicating it might be a consequence of accumulated damage.

Although DOLs were found in proximity to Aβ-plaques, their appearance long after plaque accumulation, together with our in vitro results that revealed that amyloid beta by itself is not sufficient to induce them, and the fact they were also found in models that do not exhibit amyloidosis argue against Aβ as a sufficient trigger of this cellular state. However, their presence in brain areas enriched with plaques suggests an involvement of additional factors, such as damage-associated molecular patterns (DAMPs)[52], the release of various metabolic factors from dying cells, and inflammation. Transcriptomic alterations similar to DOLs signature were also observed by spatial transcriptomics of the plaque niche[43] in a different model of amyloidosis, further supporting the notion that the plaque microenvironment is enriched in factors contributing to this cellular state.

In EAE, oligodendrocyte precursor cells (OPC) and mature oligodendrocytes with a similar signature have been shown to acquire phagocytic abilities, present antigens on MHC-II, and activate CD4 T cells[35]. In 5xFAD, unlike in EAE, by in-depth analysis of the transcriptomic profile of mature oligodendrocytes (GalC+) by scRNA-seq, we observed upregulation of MHC-I pathway only and not MHC-II, implying interaction with CD8 T cells might be more likely than with CD4 T cells. However, we cannot exclude the possibility that alterations like the ones observed in EAE are occurring in OPCs in AD. Moreover, a recent study suggested OPCs might become senescent in the context of amyloidosis[53]. In mature oligodendrocytes, we have not found evidence for any senescence markers at the transcriptomic level. However, further in-depth characterization of OPCs will be required to answer these questions. In line with our observations in the 5xFAD model, the expression level of DOL genes in EAE was found to be increased with disease progression, further supporting a relationship between damage accumulation and DOL signature expression. These observations support the general name given to this oligodendrocyte state, disease associated regardless of the nature of the etiology.

The overlap in transcriptomic signature between the DOL and disease-associated astrocytes (DAA), which were reported across several conditions[10,38,39,43,54], suggests that despite fundamental differences in function between astrocytes and oligodendrocytes, they share similar molecular pathways of response to damage (e.g. upregulation of *Serpina3n*, *C4b*, *Ctsb*). Microglial responses seem to be more pathology-specific, as in the case of DAM, which are observed in amyloidosis but not in tauopathy[9,31]. Of note, within the common signature of astrocytes and the oligodendrocytes, some genes were also found in microglia, e.g., *C4b*[55]. Further in-depth study will be required to determine the functions these responses serve and how they may be targeted in developing effective therapeutics for CNS pathologies.

Using immunohistochemistry, we detected SERPINA3$^+$ oligodendrocytes in human postmortem AD brains. Spatial transcriptomics revealed high intensity of *SERPINA3* signature associated with inflammation in proximity to macrophages, further supporting the contention that *SERPINA3* expression is potentially induced by inflammation and damage. However, the fact that we used a single marker in the immunohistochemistry and that spatial transcriptomics lacks single-cell resolution prevented us from fully characterizing these cells to determine the degree of similarity to mouse DOLs. We also showed a correlation between the proportion of SERPINA3$^+$ cells in the brain and the MMSE score, suggesting SERPINA3 may serve as a biomarker of cognitive impairment. Of note, *Serpina3n* was shown to inhibit Granzyme B[22], therefore protecting cells from cytotoxic death induced by CD8 T-cells. In addition, it was shown to promote plaque aggregation *in vitro*[11]. Therefore, further studies are necessary to elucidate the role of DOLs, and Serpina3n in particular, and their relevance to human diseases.

In summary, our work shows the common molecular pathways oligodendrocytes acquire in multifactorial, neurodegenerative conditions and emphasizes the potential of targeting these common pathological mechanisms underlying CNS diseases.

Methods

Mice

Heterozygous 5xFAD transgenic mice (on a C57/BL6-SJL background) that overexpress familial AD mutant forms of human APP (the Swedish mutation, K670N/M671L; the Florida mutation, I716V; and the London mutation, V717I) and PS1 (M146L/L286V) transgenes under the transcriptional control of the neuron-specific mouse Thy-1 promoter[17] (5XFAD line Tg6799; The Jackson Laboratory), were taken throughout adulthood in different time points as indicated in the text. Genotyping was performed by PCR analysis of tail DNA. Throughout the study, WT controls in each experiment were non-transgene littermates from the relevant mouse colonies. Mice were bred and maintained by the animal breeding center of the Weizmann Institute of Science. All experiments detailed herein complied with the regulations formulated by the Institutional Animal Care and Use Committee (IACUC) of the Weizmann Institute of Science.

Brain dissociation for single-cell suspension

Mice were euthanized using an overdose of ketamine-xylazine, followed by transcardial perfusion with cold PBS, and whole brains were excised. Tissues were chopped into small pieces and subjected to 30 minutes of enzymatic digestion using papain (Worthington, LS003127) in 37°C, followed by manual trituration using a 5ml pipette and filtering through a 70μm cell strainer. Cells were pelleted at 800g for 5 min in 4°C and then suspended in ovomucoid protease inhibitor (Worthington, LS003086) solution to stop papain activity. Cells were pelleted again in 600g, 5 min, 4°C, washed, and myelin debris was removed by 30% Percoll gradient (GE healthcare, 17-0891-01). Then, cells were pelleted and washed again and subjected to 20 min Fc block (1:200), following 30 min cell surface staining. Immediately before FACS, cells were washed, filtered through a 70μm cell strainer, suspended in sorting buffer (PBS supplemented with 0.2mM EDTA pH8 and 0.5% BSA), and DAPI was added. Samples were kept on ice at all times except for enzymatic digestion.

Single-cell sorting

Cell populations were sorted using FACS-AriaIII or FACSymphony-S6 and FACS DIVA software (BD Biosciences, San Jose, CA). For the sorting of all the non-immune populations, samples were gated for $CD45^-$ (APC, clone 30F-11, 17-0451-82, eBioscience or 103115, BioLegend, 1:200), while excluding debris (FSC-A vs. SSC-A), dead cells ($DAPI^+$), and doublets (FSC-A vs. FSC-H). In order to enrich for different cell populations, the following markers were used: GalC (oligodendrocytes, FITC, clone mGalC, FCMAB312F, Milli-Mark, 1:10), Ly6A/E (endothelial, BV605, clone D7, 108133, BioLegend, 1:150). Isolated cells were single-cell sorted into 384-well cell capture plates containing 2μl of lysis solution and barcoded poly(T) reverse-transcription (RT) primers for single-cell RNA-seq[15]. Four empty wells were kept in each 384-well plate as a no-cell control. Immediately after sorting, each plate was spun down to ensure cell immersion into the lysis solution, snap-frozen on dry ice, and stored at −80°C until processing. To record the marker level of each single cell, the FACS Diva ‘index sorting’ function was activated during single-cell sorting. Following the sequencing and analysis of the single cells, each surface marker was linked to the genome-wide expression profile. This methodology was used to optimize the gating strategy and to eliminate autofluorescent cells. No statistical methods were used to pre-determine sample sizes but our sample sizes are similar to or bigger than those reported in previous publications[9,10].

Single-cell RNA library preparation by Massively parallel Single Cell RNA sequencing (MARS-seq)

Single-cell libraries were prepared using MARS-seq 2.0 protocol[15]. Briefly, mRNA from the cells sorted into cell capture plates were barcoded, converted into cDNA, and pooled. The pooled sample was linearly amplified by T7 in vitro transcription. The resulting RNA was fragmented and converted into a sequencing-ready library by tagging the samples with pool barcodes and Illumina sequences during ligation, RT, and PCR. Each pool of cells was tested for library quality as described in MARS-seq 2.0 protocol.

Low-level processing of the scRNA-seq data

MARS-seq libraries, pooled at equimolar concentrations, were sequenced using an Illumina NextSeq 500 or NovaSeq 6000 sequencer at a sequencing depth of 20K-50K reads per cell. Reads were condensed into original molecules by counting the same unique molecular identifiers (UMI). Statistics on empty-well spurious UMI detection were used to ensure that the batches used for analysis showed a low level of cross-single-cell contamination (less than 3%). Mapping of reads was done using HISAT (version 0.1.15)[57]; reads with multiple mapping positions were excluded. Reads were associated with genes if they were mapped to an exon, using the UCSC genome browser for reference. Exons of different genes that shared genomic positions on the same strand were considered a single gene with a concatenated gene symbol.

Basic statistical analysis and visualization

Most of the variables studied in our study are not normally distributed, thus Kruskal-Wallis rank test was used to compare values between groups. As Kruskall-Wallis test is a non-parametric one, data normality does not have to be checked. Ordinary least square regressions were computed using the lm() function and the p-value associated with slope was computed using the summary() function. Quality of the linear models were visually checked for any possible bias. Correction for multiple testing was done using Benjamini Hochberg correction implemented in the p.adjust() function when necessary.

For visualization, when the number of points per group was larger than 30, the boxplot() function was used with parameters set to default except for the ‘outline’ parameter, which was set to FALSE.

ScRNA-seq data processing and clustering

ScRNA-seq expression data analysis was performed using the R-based Pagoda2 pipeline (https://github.com/hms-dbmi/pagoda2/)[18] in addition to an in-house R script. Low-quality cells were removed using the following strategy: cells with less than 350 UMIs and more than 30% of mitochondrial genes were removed. The number of Highly Variables Genes (HVGs) was determined using the adjustVariance() function with the gam parameter set to 5. HVGs were selected using the following strategy: for each gene, its number of zeros and its mean expression were computed. A local polynomial model was then used to predict the number of zeros according to the log mean expression (loess function with degree parameter set to 2). The residuals of this model (excess of zeros) were then used to rank the genes, and the genes with the highest excess of the zeros were considered the most HVGs. PCA reduction was then computed using the calculatePcaReduction() function. The number of computed PC was changed in each analysis due to a variable number of cells and cellular heterogeneity. A K-nearest neighbor graph was then built with the function makeKnnGraph() with the K value set to 30 and the distance parameter set to 'cosine'. Clusters were computed using the Louvain's clustering approach implemented in the getKnnClusters() and multilevel.community() functions. Marker genes were identified using the getDifferentialGenes() function. UMAP low dimensional embedding was computed using the uwot R package, and more precisely the umap() function with the n_neighbors parameter set to 30 and the metric parameter set to 'cosine'. In order to group clusters of cells in the first round of analysis, mean gene expression of the most variable genes was computed using the aggregate() function. Spearman's correlation matrix was computed using the cor() function with the method parameter set to 'Spearman'. Hierarchical clustering was then performed on this matrix using Ward's method and the resulting tree was used to aggregate the cell clusters. Data collection and analysis were not performed blind to the conditions of the experiments.

Single-cell differential gene expression analysis and power analysis

To perform differential expression analysis, a dichotomized-based approach was used as previously described[19]. Briefly, gene expression was first dichotomized (if the normalized expression was bigger than 0, the gene was considered as expressed) and then a binomial Generalized Linear Model (GLM) was computed with a complementary log log link function (cloglog) using the glm() R function. To mitigate the effect of library size variation across the cells, it was included as a covariate in the model. The corresponding P-values were computed using a Likelihood Ratio Test (LRT) and then corrected using Benjamini Hochberg correction.

Power analysis was performed by randomly sampling 15 times a given proportion of the oligodendrocytes (80%, 70%, 60%, 50%, 20%, 10%, and 5%) and then performing the dichotomized gene expression analysis described above.

Poisson Regression for the analysis of cluster abundancy

Robust detection of cell clusters that were differentially abundant between WT and 5xFAD mice was performed for oligodendrocytes cluster using a Poisson regression where the observed variable is the number of oligodendrocytes belonging to this cluster in each mouse and the explanatory variables are the total number of cells sequenced from each mouse, and the genotype of the mouse (5xFAD or WT). This model was fitted using the glm() R core function. An exponential link function was used, and the total number of cells was therefore logged. P-values were corrected using Benjamini Hochberg correction, implemented in the p.adjust() function.

Promoter motif analysis

Promoter analysis was performed using iRegulon[28] (Cytoscape plugin, version 1.3). The 'Species and gene nomenclature' parameter was set to 'Mus musculus, MGI symbols', and only motifs 500 base-pairs upstream of the Transcription Start Sites (TSS) were used. All other parameters were set to default values.

Gene Set Enrichment Analysis (GSEA)

GSEA was performed using the liger (version 1.12) and the gskb (version 1.16)[58] packages. Briefly, a gene set describing a list of biological pathways was loaded (mm_pathway object) from the gskb library and then used to analyze the log2FC value list using the bulk.gsea() function from liger.

Meta-analysis of previously published scRNA-seq

The dataset containing the P301L and the PS2/APP/P301L and the two EAE datasets used in the meta-analysis were downloaded from Gene Expression Omnibus (GEO) server by the following accession numbers: P301L and the PS2/APP/P301L- GSE153895, acute EAE-GSE113973, multiphasic EAE- GSE118257. Annotations of the samples were done using the getGEO() function from the GEOquery package (version 2.48). The aging SVZ 10x scRNA-seq data were kindly provided by the authors. Expression data were processed using the same approach as described above. A cell cluster was considered corresponding to oligodendrocytes if it specifically expressed a known oligodendrocyte marker such as Plp1 or Mbp.

Primary oligodendrocyte cultures

Primary oligodendrocyte-precursor cells (OPC) were cultured as follows: P0-3 mouse pups were decapitated, cortices were extracted and put in DMEM+penicillin/streptomycin media on ice. Then, cortices were homogenized by two triturations with 19G needle, followed by two triturations with 21G needle. Then, the suspension was centrifuged (200g, 5 min, room temp), suspended in Glia medium (DMEM, 10% heat-inactivated fetal bovine serum, 5% heat-inactivated horse serum, penicillin/streptomycin), and seeded in flasks. Glia medium was replaced every three days, and from the sixth day, insulin (5ul/ml, Sigma l6634) was supplied. After ten days, flasks were gently knocked, and media was removed to remove microglia, followed by shaking overnight in 250RPM at 37°C. The following day, OPCs were purified from the supernatant using MACS separation O4 beads (130-096-670, Miltenyi Biotec) and seeded over poly-D-lysine, poly-L-ornithine pre-coated plates. OPCs were grown in DMEM supplemented with horse serum, B-27, pyruvate, penicillin/streptomycin, Glutamax, T3, and T4. Media was replaced every two days.

Culture stimulation, bulk RNA purification, and library preparation

Oligodendrocytes were stimulated upon maturation. For Aβ stimulation, different aggregation states were prepared from HFIP-treated $A\beta_{1\text{-}42}$ (Bachem 4090148) as previously described[32]. Scrambled Aβ was used as control (Bachem 4064853). Cells were treated with aggregated Aβ at 20nM concentration for 24h. Cells were collected, and mRNA was purified using Dynabeads mRNA purification kit (Invitrogen). Libraries were prepared using a modified MARS-seq protocol for bulk.

Analysis of bulk RNA-seq data

Bulk sequencing data were analyzed using DESeq2 (version 1.24)[59] and apeglm (version 1.60)[60] packages. Samples with less than $2*10^5$ UMIs sequenced and genes with less than 50 total UMIs were removed from the analysis. A DESeq2 object was created using the dds() function. The underlying statistical model was fit using the DESeq() function with parameter 'fitType' set to 'parametric'. Due to the low number of technical replicates used in each experiment (3 samples per condition), the shrank log2 fold changes were computed using the lfcShrink function with the parameter 'type' set to 'apeglm'.

Immunofluorescence and imaging

For mouse immunofluorescence, mice were euthanized, intracardially perfused with PBS, and brains were extracted and fixed in paraformaldehyde 2.5% overnight, then washed with PBS and immersed in 30% sucrose until sinking. 30µm free-floating brain sections were cut using a sliding microtome (Leica) and quenched using 100mM NH_4Cl for 1 hour at room temperature, blocked in PBS with 10% donkey serum and 0.5% Triton and then stained using the following primary antibodies: Olig2 (AB9610, Merck, 1:200), Serpina3n (AF4709, R&D Systems, 1:200), hAβ (BLG-803001, BioLegend, 1:200) in PBS with 5% donkey serum and 0.1% Triton. Secondary antibodies used were donkey anti-rabbit cy2 (Jackson ImmunoResearch #711-225-152, 1:200), donkey anti-goat cy3 (Jackson ImmunoResearch #705-165-147, 1:200) and donkey anti-mouse cy5 (Jackson ImmunoResearch #715-175-151, 1:200). For human immunofluorescence, paraffin-embedded human brain temporal cortex sections of postmortem Alzheimer's disease and non-demented, aged-matched individuals were obtained from the Oxford Brain Bank (formerly known as the Thomas Willis Oxford Brain Collection (TWOBC)) with appropriate consent and Ethics Committee approval by the Weizmann Institutional Review Board (IRB). Following de-paraffinization, antigen retrieval was performed in Tris-EDTA (pH=9). Sudan black (0.1%) treatment was performed prior to staining to reduce autofluorescence. Aβ staining was done by Thioflavin-S (1%), followed by primary antibodies: CC1 (ab16794, Abcam, 1:50), SERPINA3 (ab205198, Abcam, 1:100). Secondary antibodies used were donkey anti-rabbit cy5 (Jackson ImmunoResearch #711-175-152, 1:200) and donkey anti-mouse cy3 (Jackson ImmunoResearch #715-165-150, 1:200). Representative images were captured using a confocal microscope (LSM 880, 20x and 63x lens), and Zeiss ZEN software was used for image capturing. Representative images were merged and optimized using Adobe Photoshop. For DOLs quantification (human, mouse) and plaque association (mouse), Olympus BX61VS slide scanner and VA-ASW-S6 software were used. For oligodendrocyte culture bright field image, Olympus IC70 microscope with XM10 CCD camera was used.

Image processing

Analysis was conducted on raw images. All image processing steps (segmentation, quantification) were performed using Python version 3.9 in a Jupyter Notebook. Cells were first segmented using the Mesmer tool from the python DeepCell package[40]. The nuclear segmentation mode was used (im.compartment =‘nuclear’) on the DAPI channel, and the resulting masks were extended using the expand_labels() function from the skimage package using a 5-pixel radius disk as a mask. To identify the plaques, a Laplacian of Gaussian transform was applied to the Aβ channel by first applying a gaussian filter of size 50 (Gaussian function from the skimage package) and then applying a discrete Laplacian filter (laplace function). The resulting image was thresholded using Otsu’s automated thresholding, implemented by the threshold_otsu() from the skimage package, and watershed segmentation was used. Briefly, a distance map was computed from the binary image using the distance_transform_edt() function from the scipy package and local peaks extracted with the corner_peaks() function from the skimage package with the following parameter values : footprint = np.ones((10,10)), min_distance = 20 and exclude_border =False. The final step of the watershed was then performed using the watershed() function from skimage. The various properties of the identified cells and plaques (size, location, mean marker expression) were computed using the regionprops_table() function from the skimage package and then exported as a text file.

Spatial analysis

The analysis of the resulting image segmentation/processing steps was solely performed on R 4.0.3. Automated thresholding of the fluorescence intensity was performed using Otsu’s thresholding method, implemented by an in-house script. As the intensity distribution was highly heavy-tailed for the human samples, a cubic root transform was applied to get a more ‘normal-like’ distribution before performing the thresholding. The normalized Besag’s L functions were computed using the Linhom() function from the Spatstat package. To get the normalized version of this function, the theoretical value of the function was subtracted to the estimated value.

To fit the penalized Gibbs model, the PenGe package was used (https://github.com/antiphon/PenGE): first, a spatstat object was built using the ppp() function with a default window of width 20.000 and height 6500. The model was fitted using the make_Q_stepper_multi() and fitGlbin_CV() functions. Thirty different values on a log-scale of lambda were used, and the vector of the range was set to c(100,250,500,1000,1500) (pixel scale with 3 pixels equal to one micron). The lambda with the highest log-likelihood was selected and the corresponding model was used for analysis.

Human spatial transcriptomic preprocessing

BCL files were processed with the SpaceRanger (v.1.2.2) to generate FASTQ files via spaceranger mkfastq. The FASTQ file was then aligned and quantified based on the reference GRCh38 Reference-2020-A via spaceranger count. The functions spaceranger mkfastq and spaceranger count were used for demultiplexing sample and transcriptome alignment via the default parameter settings. Sctransform[61] (v.0.3.2) was used to normalize the raw count data for the following analysis based on default parameters.

Spatial transcriptomic data analysis

Spatial transcriptomic data were processed using the following approach: first low-quality spots having less than 1000 UMIs were filtered out. Using the pagoda2 pipeline, the 1000 most variable genes were selected using the r$adjustVariance() function. Then, using the CountClust package, a Latent Dirichlet Allocation (LDA) analysis was performed (FitGoM() function) using five different number of topics (10, 15, 20, 25, and 30 topics) and with 'tolerance' parameter set to 100. The model displaying the lowest BIC score was selected and used for further analysis.

In order to identify biologically meaningful genes, the contribution table obtained from the FitGoM function was normalized by applying the following transformation to the contribution cij of each gene i and for each topic j:

$$\text{cij'} = \lambda * \log(\text{cij}) + (1\text{-}\lambda) * \log(\text{cij} / \text{Si})$$

Where cij' is the normalized contribution of gene i for topic j, λ a parameter set to 0.5 and Si the contribution of gene i to the total number of UMIs.

Extended Data

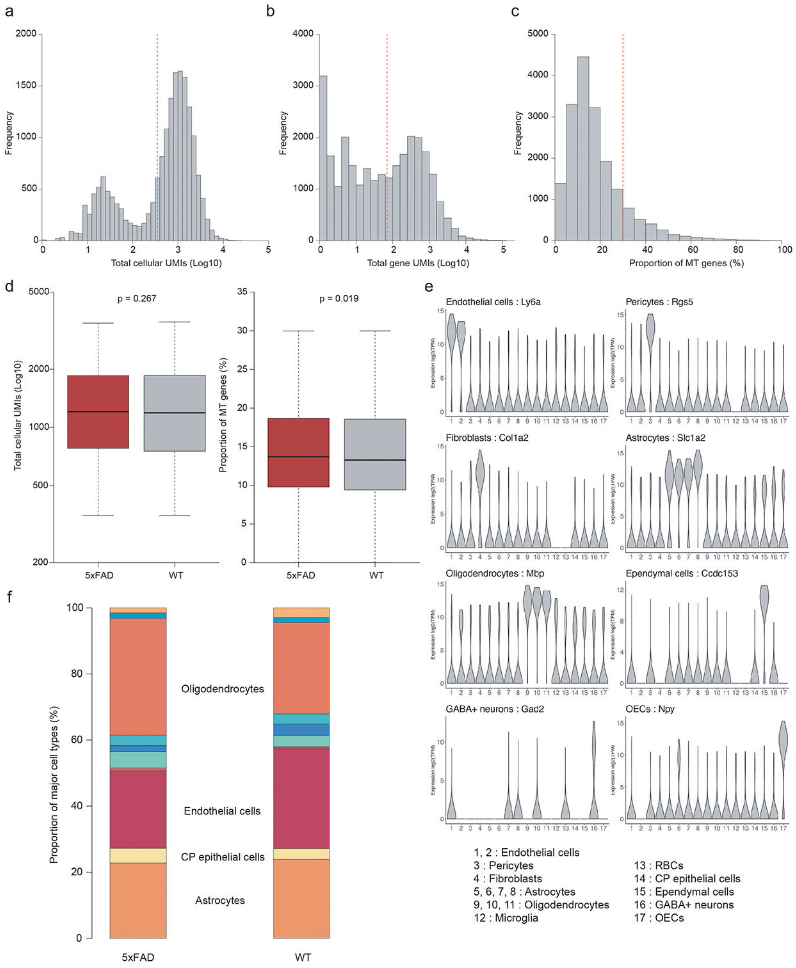

Extended Data Fig. 1. Quality control of CD45-libraries described in figure 1

Extended data Figure 1 associated to Figure 1. (a) Distribution of total cellular unique molecular identifiers (UMI). Dashed line marks the threshold for analysis. (b) Distribution of total gene UMIs. Dashed line marks the threshold for analysis. (c) Distribution of the proportion of mitochondrial genes. Dashed line marks the threshold for analysis. (d) Comparison of the total cellular UMI distribution in cells from 5xFAD and WT mice (left panel) and the proportion of mitochondrial genes in cells from 5xAD and WT mice (right panel). P-values were computed using a Kruskal-Wallis test. The box bounds the IQR. Line, median. Whiskers extend to a maximum of 1.5*IQR beyond the box. n=18 independent mice (9 5xFAD, 9 WT) (e) Violin plot of known marker genes expression across the different cell clusters. (f) Comparison of the main cell-type proportions between 5xAD and WT mice.

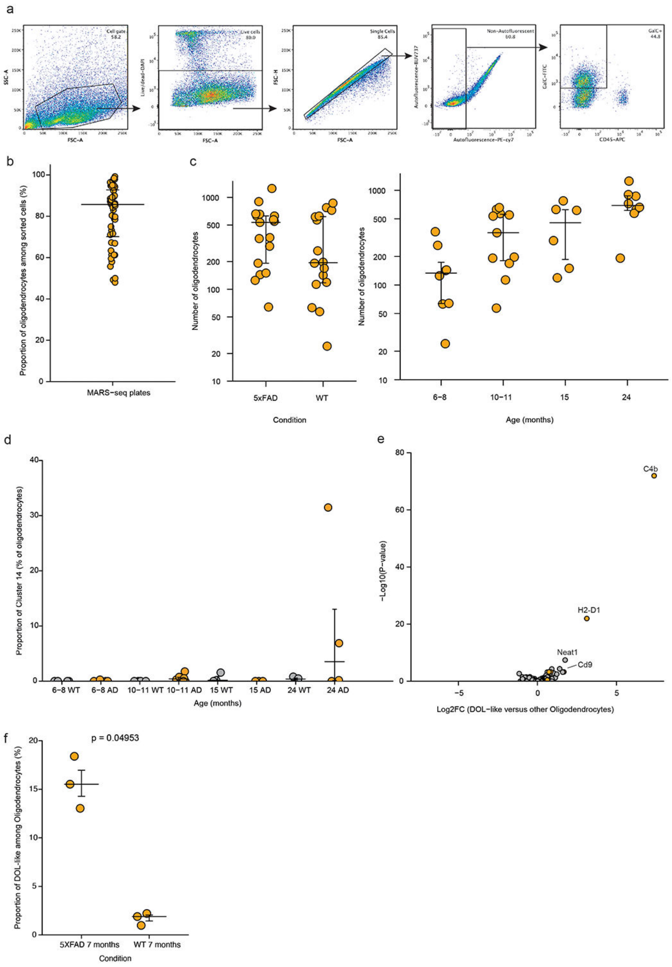

Extended Data Fig. 2. Quality control of GalC+ libraries described in figure 2

Extended data Figure 2 associated to Figure 2. (a) Gating strategy used to enrich for oligodendrocytes. (b) Proportion of oligodendrocytes isolated in each sequenced plate. Large bars correspond to the median and small bars to IQR. n=48 384-well plates (c) Number of oligodendrocytes sequenced for each 5xAD and WT mice (left panel) and across ages (right panel). Large bars correspond to the median and small bars to IQR. n=33 independent mice (17 5xFAD, 16 WT) (d) Proportion of cluster 14 in WT and 5xFAD mice across ages. Large bars correspond to the median and small bars to IQR. n=33 independent mice (across ages: 6-8m; n=4 5xFAD, 4 WT, 10-11m; n=6 5xFAD, 5 WT, 15m; n=3 5xFAD, 3 WT, 24m; n=4 5xFAD, 4 WT) (e) Volcano plot corresponding to the differential expression analysis between DOL-like and the rest of oligodendrocytes as identified by Zhou et al.11. DOL genes are colored in orange. (f) Proportion of DOL-like among oligodendrocytes between 5xFAD and WT mice in the data by Zhou et al.11. P-value was computed using the Kruskal-Wallis test.

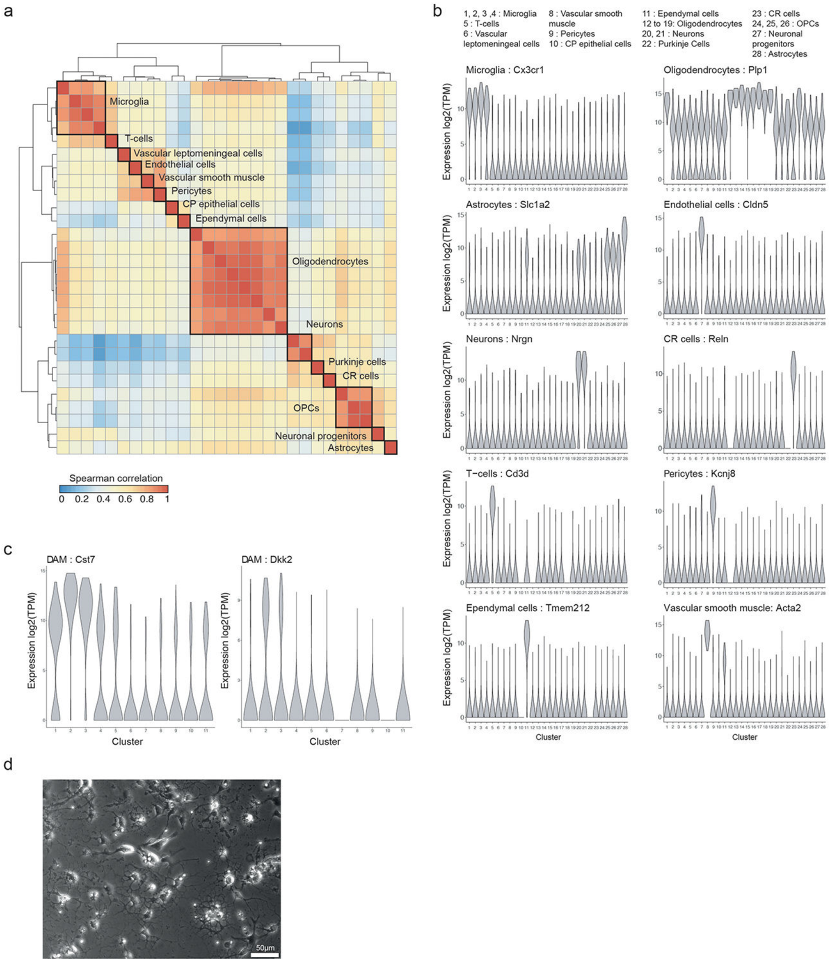

Extended Data Fig. 3. Cell type annotation of dataset described in figure 3 and culture quality control

Extended data Figure 3 associated to Figure 3. (a) Spearman correlation between the mean transcriptomic profiles of the cell clusters identified in the dataset from Lee et al. (b) Violin plot of known marker genes across the different cell clusters. (c) Violin plot of known DAM marker gene expression across the different microglia clusters after refined clustering. (d) Representative bright-field microscopy image of the primary oligodendrocyte culture; scale bar corresponds to 50μm. Representative results from 12 independent experiments.

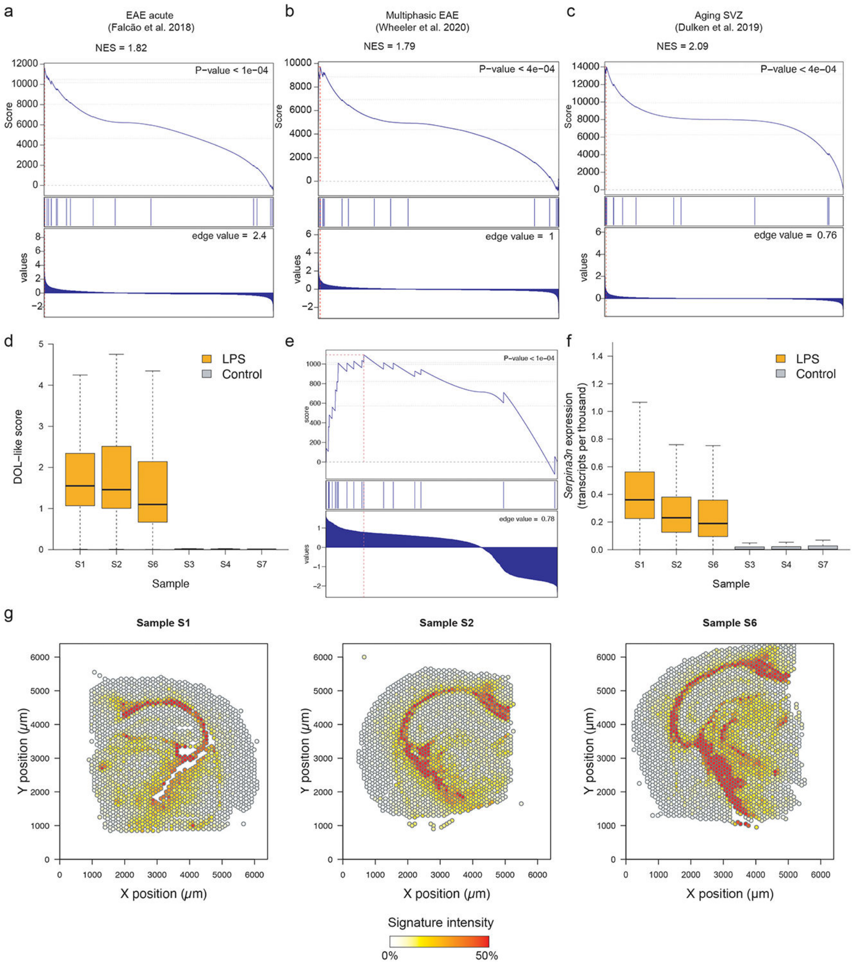

Extended Data Fig. 4. GSEA and quality control of datasets described in figure 4

Extended data Figure 4 associated to Figure 4. **(a)** GSEA analysis plot corresponding to the acute EAE dataset. **(b)** GSEA analysis plot corresponding to the multiphasic EAE dataset. **(c)** GSEA analysis plot corresponding to the aging SVZ dataset. **(d)** score of topic number 8, corresponding to DOL-like signature, in LPS-stimulated and control samples. n=6 independent samples (3 LPS-stimulated, 3 control). Thick line corresponds to the median, the bottom and upper limits of the box to the first and third quartile, respectively. The lower and upper whiskers correspond to the lowest and highest values respectively within the range of the first (third) quartile minus (plus) 1.5 times the Interquartile range. **(e)** GSEA analysis plot of the DOL signature in topic 8. **(f)** *Serpina3n* expression (transcripts per thousand) in LPS-treated and control mice. n=6 independent samples (3 LPS-stimulated, 3 control). p-value was computed by performing a Gene Set Enrichment Analysis as described by Subramanian et al[56]. Thick line corresponds to the median, the bottom and upper limits of the box to the first and third quartile, respectively. The lower and upper whiskers correspond to the lowest and highest values respectively within the range of the first (third) quartile minus (plus) 1.5 times the Interquartile range. **(g)** Intensity of the oligodendrocyte signature across the sections of the three LPS treated mice.

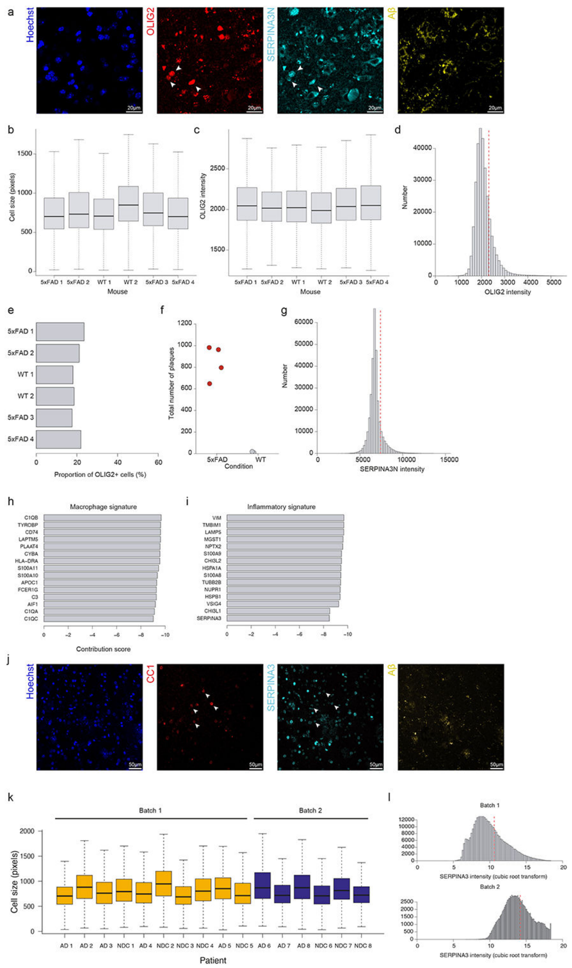

Extended Data Fig. 5. Quality control of image analysis described in figure 5

Extended data Figure 5 associated to Figure 5. **(a)** Separated channels corresponding to the 5xFAD brain sample in fig. 5a; scale bar corresponds to 20µm. **(b)** Distribution of cell size across mice samples. The box bounds the IQR. Line, median. Whiskers extend to a maximum of 1.5*IQR beyond the box. n=6 independent samples (4 5xFAD, 2 WT). **(c)** Distribution of OLIG2 intensity across mouse samples. The box bounds the IQR. Line, median. Whiskers extend to a maximum of 1.5*IQR beyond the box. n=6 independent samples (4 5xFAD, 2 WT). **(d)** Distribution of OLIG2 intensity and estimated threshold (vertical red line). **(e)** Proportion of OLIG2+ cells across mouse samples. **(f)** Number of plaques in 5xFAD (n=4) and WT (n=2) mice. **(g)** Distribution of SERPINA3N intensity and the estimated threshold (vertical red line). **(h)** The 15 most contributing genes to the macrophage signature. **(i)** The 15 most contributing genes to the inflammatory signature. **(j)** Separated channels corresponding to the postmortem AD brain sample in fig. 5i; scale bar corresponds to 50µm. **(k)** Distribution of cell size across human samples. The box bounds the IQR. Line, median. Whiskers extend to a maximum of 1.5*IQR beyond the box. n=16 independent samples (8 AD, 8 NDC). **(l)** Distribution of SERPINA3 intensity and the estimated threshold (vertical red line) for the two different batches of samples.

Supplementary Material

Refer to Web version on PubMed Central for supplementary material.

Acknowledgements

The research of I.A. is supported by the Seed Networks for the Human Cell Atlas of the Chan Zuckerberg Initiative, the Thompson Family Foundation Alzheimer's Research Fund and the Adelis Foundation. I.A. is an Eden and Steven Romick Professorial Chair, supported by the HHMI International Scholar Award, the European Research Council Consolidator Grant (no. 724471-HemTree2.0), an MRA Established Investigator Award (no. 509044), DFG (no. SFB/TRR167), the Ernest and Bonnie Beutler Research Program for Excellence in Genomic Medicine, the Helen and Martin Kimmel awards for innovative investigation, and the SCA award of the Wolfson Foundation and Family Charitable Trust. Research in the M.S. lab is supported by Advanced European Research Council grants (741744); Israel Science Foundation (ISF)-research grant no. 991/16; and ISF-Legacy Heritage Bio-Medical Science Partnership-research grant no. 1354/15. We wish to thank the Adelis and Thompson Foundations for their generous support of our AD research. This work is also supported by awards K01-AG056673 and R56-AG066782-01 (H.F.) from the National Institute on Aging of the National Institutes of Health, the award R01-GM131399 (Q.M.) from the National Institute of General Medical Sciences, the award of AARF-17-505009 (H.F.) from the Alzheimer's Association, and the W81XWH1910309 (H.F.) from the Department of Defense.

Data availability statement

Raw and processed mouse sequencing data that support the findings of this study have been deposited in the Gene Expression Omnibus database under accession number GSE202297.

Code availability statement

All the code is available on Github at: https://github.com/PierreBSC/DOL_project

References

1. Masters CL et al. Alzheimer's disease. Nature Reviews Disease Primers 1, 1–18 (2015).
2. Holtzman DM, Morris JC & Goate AM Alzheimer's disease: The challenge of the second century. Science Translational Medicine 3, 77sr1–77sr1 (2011). [PubMed: 21471435]
3. Reitz C & Mayeux R Alzheimer disease: Epidemiology, diagnostic criteria, risk factors and biomarkers. Biochem. Pharmacol 88, 640–651 (2014). [PubMed: 24398425]
4. Karch CM & Goate AM Alzheimer's Disease Risk Genes and Mechanisms of Disease Pathogenesis. Biol. Psychiatry 77, 43–51 (2015). [PubMed: 24951455]
5. Schwartz M & Deczkowska A Neurological Disease as a Failure of Brain–Immune Crosstalk: The Multiple Faces of Neuroinflammation. Trends Immunol. 37, 668–679 (2016). [PubMed: 27616557]
6. Heneka MT et al. Neuroinflammation in Alzheimer's disease. Lancet Neurol. 14, 388–405 (2015). [PubMed: 25792098]
7. Wyss-Coray T & Rogers J Inflammation in Alzheimer Disease—A Brief Review of the Basic Science and Clinical Literature. Cold Spring Harb. Perspect. Med 2, a006346 (2012). [PubMed: 22315714]
8. De Strooper B & Karran E The Cellular Phase of Alzheimer's Disease. Cell 164, 603–615 (2016). [PubMed: 26871627]
9. Keren-Shaul H et al. A Unique Microglia Type Associated with Restricting Development of Alzheimer's Disease. Cell 169, 1276–1290.e17 (2017). [PubMed: 28602351]
10. Habib N et al. Disease-associated astrocytes in Alzheimer's disease and aging. Nat. Neurosci 23, 701–706 (2020). [PubMed: 32341542]
11. Zhou Y et al. Human and mouse single-nucleus transcriptomics reveal TREM2-dependent and TREM2-independent cellular responses in Alzheimer's disease. Nat. Med 26, 131–142 (2020). [PubMed: 31932797]

12. Nasrabady SE, Rizvi B, Goldman JE & Brickman AM White matter changes in Alzheimer's disease: a focus on myelin and oligodendrocytes. Acta Neuropathol. Commun 6, 22 (2018). [PubMed: 29499767]
13. Wu Y et al. Alterations of myelin morphology and oligodendrocyte development in early stage of Alzheimer's disease mouse model. Neurosci. Lett 642, 102–106 (2017). [PubMed: 28174059]
14. Behrendt G et al. Dynamic changes in myelin aberrations and oligodendrocyte generation in chronic amyloidosis in mice and men. Glia 61, 273–286 (2013). [PubMed: 23090919]
15. Keren-Shaul H et al. MARS-seq2.0: an experimental and analytical pipeline for indexed sorting combined with single-cell RNA sequencing. Nat. Protoc 1 (2019). doi:10.1038/s41596-019-0164-4
16. Jaitin DA et al. Massively Parallel Single-Cell RNA-Seq for Marker-Free Decomposition of Tissues into Cell Types. Science (80-.) 343, 776–779 (2014).
17. Oakley H et al. Intraneuronal beta-Amyloid Aggregates, Neurodegeneration, and Neuron Loss in Transgenic Mice with Five Familial Alzheimer's Disease Mutations: Potential Factors in Amyloid Plaque Formation. J. Neurosci 26, 10129–10140 (2006). [PubMed: 17021169]
18. Lake BB et al. Integrative single-cell analysis of transcriptional and epigenetic states in the human adult brain. Nat. Biotechnol 36, 70–80 (2018). [PubMed: 29227469]
19. Bost P et al. Host-Viral Infection Maps Reveal Signatures of Severe COVID-19 Patients. Cell 181, 1475–1488.e12 (2020). [PubMed: 32479746]
20. Robinson AP, Rodgers JM, Goings GE & Miller SD Characterization of oligodendroglial populations in mouse demyelinating disease using flow cytometry: Clues for MS pathogenesis. PLoS One 9, e107649 (2014). [PubMed: 25247590]
21. Vicuña L et al. The serine protease inhibitor SerpinA3N attenuates neuropathic pain by inhibiting T cell–derived leukocyte elastase. Nat. Med 21, 518–523 (2015). [PubMed: 25915831]
22. Haile Y et al. Granzyme B-inhibitor serpina3n induces neuroprotection in vitro and in vivo. J. Neuroinflammation 12, 157 (2015). [PubMed: 26337722]
23. Gadani SP, Walsh JT, Smirnov I, Zheng J & Kipnis J The Glia-Derived Alarmin IL-33 Orchestrates the Immune Response and Promotes Recovery following CNS Injury. Neuron 85, 703–709 (2015). [PubMed: 25661185]
24. Bando Y et al. Kallikrein 6 secreted by oligodendrocytes regulates the progression of experimental autoimmune encephalomyelitis. Glia 66, 359–378 (2018). [PubMed: 29086442]
25. Kwon O-C et al. SGK1 inhibition in glia ameliorates pathologies and symptoms in Parkinson disease animal models. EMBO Mol. Med 13, e13076 (2021). [PubMed: 33646633]
26. Gupta A & Pulliam L Exosomes as mediators of neuroinflammation. Journal of Neuroinflammation 11, 68 (2014). [PubMed: 24694258]
27. Pascual M, Ibáñez F & Guerri C Exosomes as mediators of neuron-glia communication in neuroinflammation. Neural Regeneration Research 15, 796–801 (2020). [PubMed: 31719239]
28. Janky R et al. iRegulon: From a Gene List to a Gene Regulatory Network Using Large Motif and Track Collections. PLoS Comput. Biol 10, e1003731 (2014). [PubMed: 25058159]
29. Hashimoto R et al. Origins of oligodendrocytes in the cerebellum, whose development is controlled by the transcription factor, Sox9. Mech. Dev 140, 25–40 (2016). [PubMed: 26940020]
30. Stolt CC et al. The Sox9 transcription factor determines glial fate choice in the developing spinal cord. Genes Dev. 17, 1677–1689 (2003). [PubMed: 12842915]
31. Lee S-H et al. Trem2 restrains the enhancement of tau accumulation and neurodegeneration by β-amyloid pathology. Neuron 109, 1283–1301.e6 (2021). [PubMed: 33675684]
32. Stine WB, Jungbauer L, Yu C & Ladu MJ Preparing synthetic Aβ in different aggregation states. Methods Mol. Biol 670, 13–32 (2011). [PubMed: 20967580]
33. Constantinescu CS, Farooqi N, O'Brien K & Gran B Experimental autoimmune encephalomyelitis (EAE) as a model for multiple sclerosis (MS). Br. J. Pharmacol 164, 1079 (2011). [PubMed: 21371012]
34. Rangachari M & Kuchroo VK Using EAE to better understand principles of immune function and autoimmune pathology. J. Autoimmun 45, 31–39 (2013). [PubMed: 23849779]
35. Falcão AM et al. Disease-specific oligodendrocyte lineage cells arise in multiple sclerosis. Nat. Med 24, 1837–1844 (2018). [PubMed: 30420755]

36. Wheeler MA et al. MAFG-driven astrocytes promote CNS inflammation. Nature 578, 593–599 (2020). [PubMed: 32051591]
37. Dulken BW et al. Single-cell analysis reveals T cell infiltration in old neurogenic niches. Nature 1 (2019). doi:10.1038/s41586-019-1362-5
38. Liddelow SA et al. Neurotoxic reactive astrocytes are induced by activated microglia. Nature 541, 481–487 (2017). [PubMed: 28099414]
39. Hasel P, Rose IVL, Sadick JS, Kim RD & Liddelow SA Neuroinflammatory astrocyte subtypes in the mouse brain. Nat. Neurosci 2021 2410 24, 1475–1487 (2021). [PubMed: 34413515]
40. Greenwald NF et al. Whole-cell segmentation of tissue images with human-level performance using large-scale data annotation and deep learning. bioRxiv 2021.03.01.431313 (2021). doi:10.1101/2021.03.01.431313
41. Illian J, Penttinen A, Stoyan H & Stoyan D Statistical Analysis and Modelling of Spatial Point Patterns. Statistical Analysis and Modelling of Spatial Point Patterns (John Wiley, 2008). doi:10.1002/9780470725160
42. Nagele RG et al. Contribution of glial cells to the development of amyloid plaques in Alzheimer's disease. Neurobiol. Aging 25, 663–674 (2004). [PubMed: 15172746]
43. Chen WT et al. Spatial Transcriptomics and In Situ Sequencing to Study Alzheimer's Disease. Cell 182, 976–991.e19 (2020). [PubMed: 32702314]
44. Serrano-Pozo A, Betensky RA, Frosch MP & Hyman BT Plaque-associated local toxicity increases over the clinical course of Alzheimer disease. Am. J. Pathol 186, 375–384 (2016). [PubMed: 26687817]
45. Yin Z et al. Immune hyperreactivity of Aβ plaque-associated microglia in Alzheimer's disease. Neurobiol. Aging 55, 115–122 (2017). [PubMed: 28434692]
46. Griciuc A et al. TREM2 Acts Downstream of CD33 in Modulating Microglial Pathology in Alzheimer's Disease. Neuron 103, 820–835.e7 (2019). [PubMed: 31301936]
47. Rajala T, Murrell DJ & Olhede SC Detecting multivariate interactions in spatial point patterns with Gibbs models and variable selection. J. R. Stat. Soc. Ser. C Appl. Stat 67, 1237–1273 (2018).
48. Mathys H et al. Single-cell transcriptomic analysis of Alzheimer's disease. Nature 570, 332–337 (2019). [PubMed: 31042697]
49. Thrupp N et al. Single-Nucleus RNA-Seq Is Not Suitable for Detection of Microglial Activation Genes in Humans. Cell Rep. 32, 108189 (2020). [PubMed: 32997994]
50. Chen S et al. Spatially resolved transcriptomics reveals unique gene signatures associated with human temporal cortical architecture and Alzheimer's pathology. bioRxiv 2021.07.07.451554 (2021). doi:10.1101/2021.07.07.451554
51. Bin JM, Harris SN & Kennedy TE The oligodendrocyte-specific antibody 'CC1' binds Quaking 7. J. Neurochem 139, 181–186 (2016). [PubMed: 27454326]
52. Venegas C & Heneka MT Danger-associated molecular patterns in Alzheimer's disease. J. Leukoc. Biol 101, 87–98 (2017). [PubMed: 28049142]
53. Zhang P et al. Senolytic therapy alleviates Aβ-associated oligodendrocyte progenitor cell senescence and cognitive deficits in an Alzheimer's disease model. Nat. Neurosci 22, 719–728 (2019). [PubMed: 30936558]
54. Zamanian JL et al. Genomic Analysis of Reactive Astrogliosis. J. Neurosci 32, 6391–6410 (2012). [PubMed: 22553043]
55. Deczkowska A et al. Mef2C restrains microglial inflammatory response and is lost in brain ageing in an IFN-I-dependent manner. Nat. Commun 8, 1–13 (2017). [PubMed: 28232747]
56. Subramanian A et al. Gene set enrichment analysis: A knowledge-based approach for interpreting genome-wide expression profiles. (2005).
57. Kim D, Langmead B & Salzberg SL HISAT: a fast spliced aligner with low memory requirements. Nat. Methods 12, 357–360 (2015). [PubMed: 25751142]
58. Lai L et al. GSKB: A gene set database for pathway analysis in mouse. bioRxiv 082511 (2016). doi:10.1101/082511
59. Love MI, Huber W & Anders S Moderated estimation of fold change and dispersion for RNA-seq data with DESeq2. Genome Biol. 15, 550 (2014). [PubMed: 25516281]

60. Zhu A, Ibrahim JG & Love MI Heavy-Tailed prior distributions for sequence count data: Removing the noise and preserving large differences. Bioinformatics 35, 2084–2092 (2019). [PubMed: 30395178]

61. Hafemeister C & Satija R Normalization and variance stabilization of single-cell RNA-seq data using regularized negative binomial regression. Genome Biol. 20, 1–15 (2019). [PubMed: 30606230]

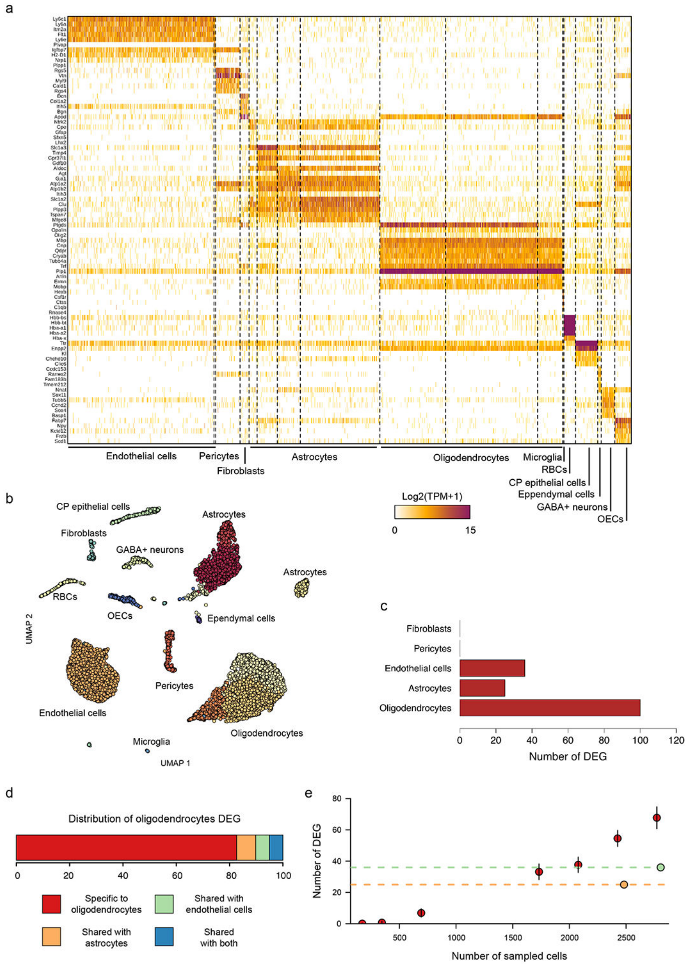

Figure 1: Oligodendrocytes display major transcriptomic alteration in the 5xFAD mouse model.

(a) Single-cell expression heatmap of non-immune (CD45^{-}) cells from 5xFAD (n=9) and WT (n=9) mice. **(b)** Two-dimensional Uniform Manifold Approximation and Projection (UMAP) embedding of the scRNA-seq data. Dots are colored based on the scRNA-seq clustering. **(c)** Number of differentially expressed genes between 5xFAD and WT mice across the major cell types. **(d)** Specificity of the differentially expressed genes in oligodendrocytes. **(e)** Power analysis- number of differentially expressed genes based on the number of cells used for the differential expression analysis. Red- down-sampling of oligodendrocytes, orange- astrocytes, green- endothelial cells. Red dots correspond to the mean number of DEG while the bar represents the standard deviation.

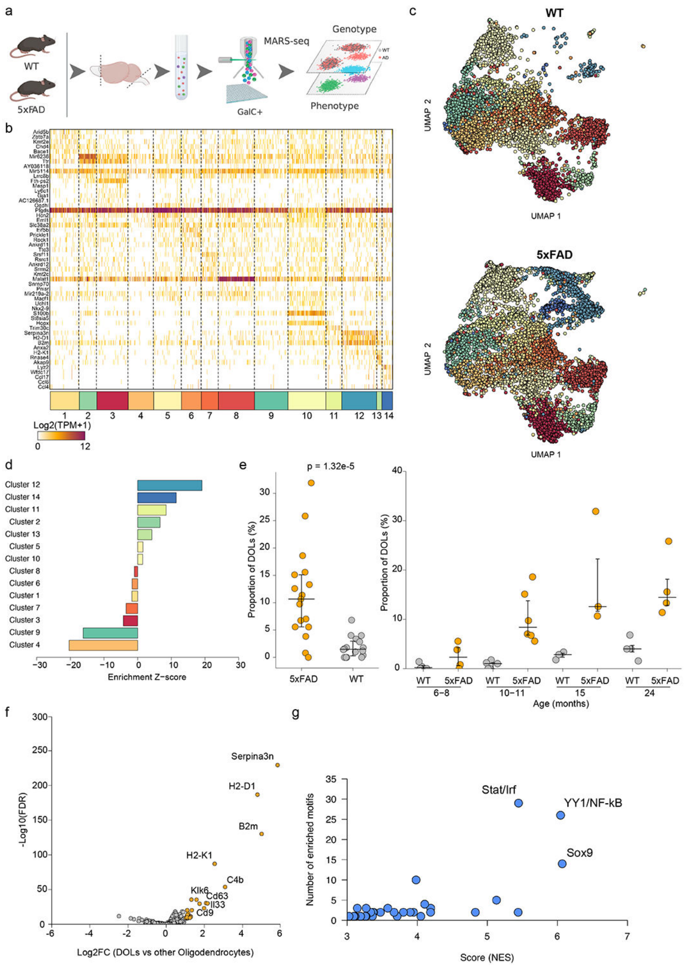

Figure 2: Identification of a disease-associated oligodendrocyte state.

(a) Experimental strategy to study oligodendrocytes. Illustration was created with Biorender.com. **(b)** Expression heatmap of oligodendrocytes from 5xFAD and WT mice at various ages, GalC$^+$ sorted and pooled together with the previously sequenced oligodendrocytes. n=33 independent mice (across ages: 6-8m; n=4 5xFAD, 4 WT, 10-11m; n=6 5xFAD, 5 WT, 15m; n=3 5xFAD, 3 WT, 24m; n=4 5xFAD, 4 WT). **(c)** Two-dimensional UMAP embedding of the scRNA-seq oligodendrocytes data. Dots are colored based on the scRNA-seq clustering. Top- cells from WT mice. bottom- cells from 5xFAD mice. **(d)** Z-score of the enrichment test comparing cluster frequency between 5xFAD and WT mice. P-values were computed by fitting a Poisson regression and corrected using multiple-testing (Methods). **(e)** Proportion of DOLs among oligodendrocytes between 5xFAD and WT mice (left panel) and across ages (right panel). P-value was computed using the Kruskal-Wallis test. Large bars correspond to the median and small bars to IQR. n=33 independent mice (across ages: 6-8m; n=4 5xFAD, 4 WT, 10-11m; n=6 5xFAD, 5 WT, 15m; n=3 5xFAD, 3 WT, 24m; n=4 5xFAD, 4 WT) **(f)** Volcano plot corresponding to the differential expression analysis between DOLs and the rest of the oligodendrocytes. **(g)** Results of the promoter analysis by iRegulon.

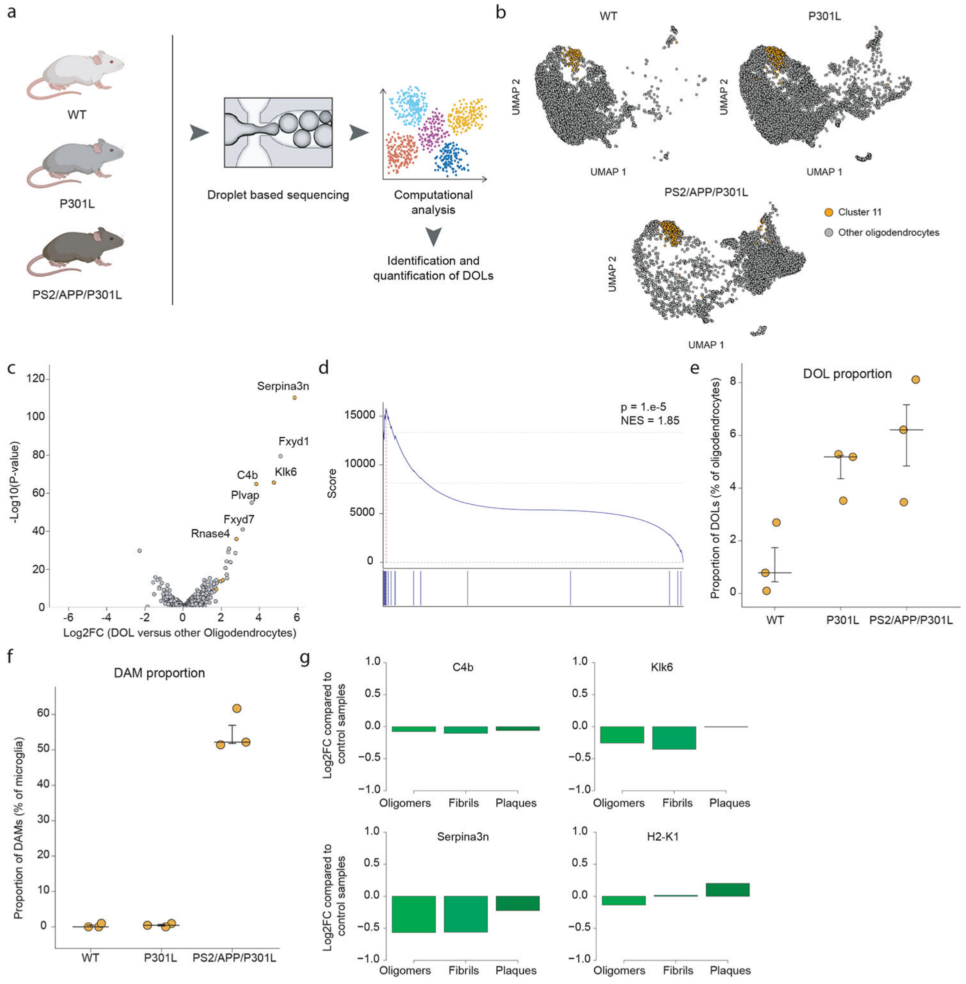

Figure 3: DOLs are independent of dementia's etiology.

(a) Experimental strategy in the scRNA-seq dataset from Lee et al.[31] **(b)** Two-dimensional UMAP embedding of the oligodendrocytes in each mouse model. Cluster 11 cells are in orange . **(c)** Comparison of the mean transcriptional profile of oligodendrocytes from cluster 11 with the rest of the oligodendrocytes. DOL genes are colored in orange. **(d)** Result of GSEA analysis performed on the log2FC list between oligodendrocytes from cluster 11 and the rest of the oligodendrocytes using the DOL genes as a query gene set. p-value was computed by performing a Gene Set Enrichment Analysis as described by Subramanian et al[56]. **(e)** Proportion of DOLs among oligodendrocytes across mouse strains (n=3 for each strain). Large bars correspond to the median and small bars to IQR. **(f)** Proportion of DAM among microglia across mouse strains. (n=3 for each strain). Large bars correspond to the median and small bars to IQR. **(g)** Log2FC of DOL genes in cultured oligodendrocytes after treatment with Aβ at different aggregation stages.

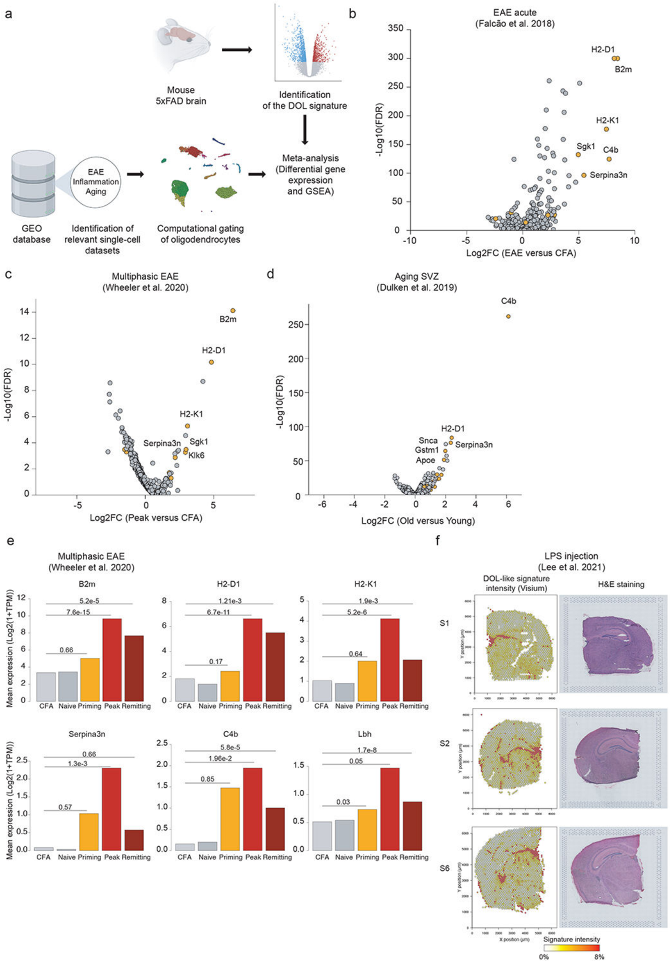

Figure 4: DOL signature in non-AD pathologies.

(a) Analytical approach used to identify DOL signature in additional CNS pathologies. **(b)** Volcano plot corresponding to the differential expression analysis between oligodendrocytes from control (CFA) and EAE spinal cord, Falcão et al.[35]. DOL genes are colored in orange. **(c)** Volcano plot corresponding to the differential expression analysis between oligodendrocytes from control (CFA) and peak EAE spinal cord, Wheeler et al.[36]. DOL genes are colored in orange. **(d)** Volcano plot corresponding to the differential expression analysis between oligodendrocytes from control young and old mice, Dulken et al.[37]. DOL genes are colored in orange. **(e)** Kinetics of the mean expression level of key DOL genes across various EAE stages. p-values were computed using a binomial regression with complementary log-log link function (Methods). **(f)** Intensity of the DOL-like signature across the sections of the three LPS treated mice (left). H&E staining of the corresponding slides (right).

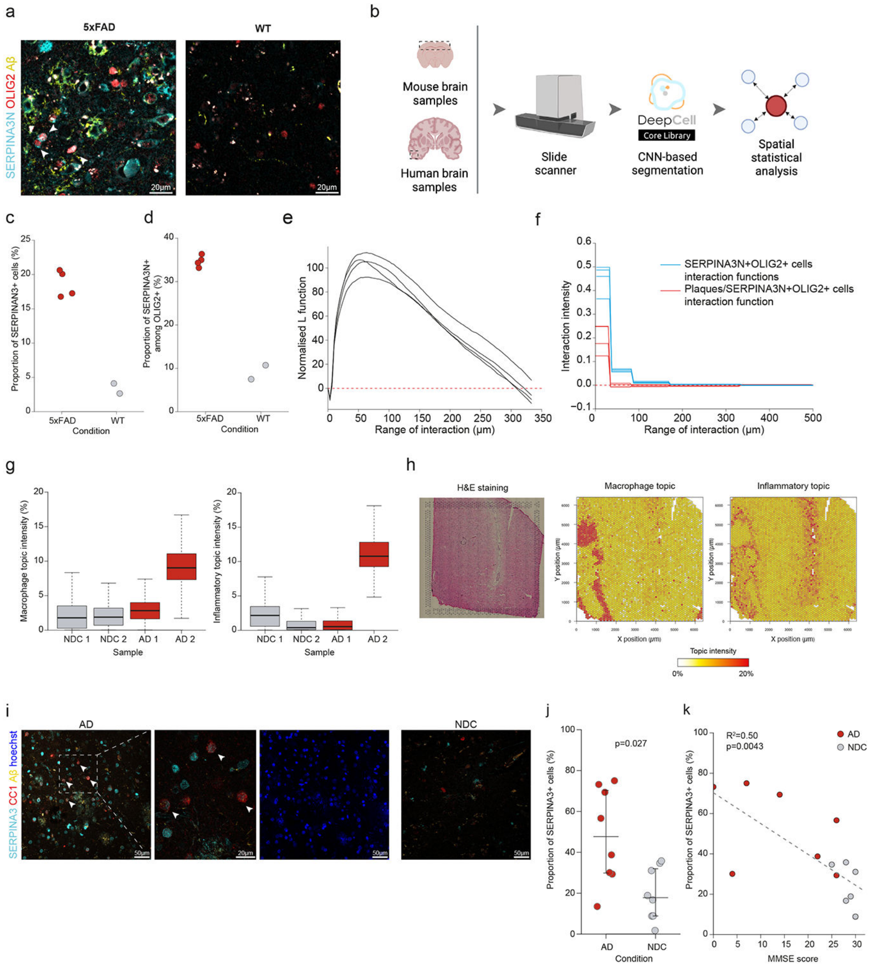

Figure 5: Spatial analysis of DOLs in mouse and human brain sections.

Immunohistochemistry of DOL-like cells and analysis of spatial association with areas enriched with plaques in 5xFAD mice **(a-f)**. **(a)** Representative image of DOLs (OLIG2+ (red) SERPINA3N+ (cyan)) from cortex of 16 months-old 5xFAD and WT mice. in 5xFAD, DOLs are in proximity to Aβ-plaques (yellow); magnification 63x, scale bar corresponds to 20μm. Arrowheads point to OLIG2+SERPINA3N+ cells. **(b)** Description of the experimental and computational approach used to study DOLs location in mouse and human brains. Illustration was created with Biorender.com. **(c)** Proportion of SERPINA3N+ cells in 5xFAD (n=4) and WT (n=2) mice. Large bars correspond to the median and small bars to IQR. **(d)** Proportion of SERPINA3N+ cells among OLIG2+ cells in 5xFAD and WT mice. Large bars correspond to the median and small bars to IQR. **(e)** Normalized L-functions of the SERPINA3N+/OLIG2+ cells in 5xFAD sections. Each curve corresponds to a unique sample. **(f)** Estimated interaction functions within SERPINA3N+/OLIG2+ cells (blue curves) or between them and plaques (red curves) in 5xFAD mice. Each curve corresponds to a unique sample. Analysis of Visium data from postmortem human AD brains **(g-h). (g)** Intensity of the macrophage (left) and inflammatory (right) topics across the four samples. n=4 biologically independent samples (2 AD, 2 NDC). Thick line corresponds to the median, the bottom and upper limits of the box to the first and third quartile, respectively. The lower and upper whiskers correspond to the lowest and highest values respectively within the range of the first (third) quartile minus (plus) 1.5 times the Interquartile range. **(h)** H&E staining of the AD2 sample (left panel), spatial pattern of the macrophage (middle panel) and inflammatory (right panel) topics. Immunohistochemistry of postmortem human AD brains **(i-k)**. **(i)** Representative image of postmortem AD patient (right) and NDC (left) temporal cortex stained for oligodendrocytes marker (CC1, red), SERPINA3 (cyan), Aβ (Thioflavin S, yellow), and nuclei (Hoechst, blue); Magnification 20x, scale bar corresponds to 50µm. Arrowheads point to CC1+SERPINA3+ cells. Inset marks position of right image in 63x magnification, scale bar corresponds to 20µm. **(j)** Proportion of SERPINA3N+ cells in AD (n=8) and NDC (n=8) samples. Large bars correspond to the median and small bars to IQR. p-value was computed using a Wilcoxon rank test. **(k)** Association between MMSE score and proportion of SERPINA3+ cells. Dashed line corresponds to an ordinary least square linear. p-value was computed by testing the significance of the contribution of the MMSE score to predict the proportion of SERPINA3+ cells using a likelihood ratio test.